Current Biology *16*, 1924–1930, October 10, 2006 DOI 10.1016/j.cub.2006.07.054

Report

A Novel Mechanism for the Formation of Actin-Filament Bundles by a Nonprocessive Formin

Alphée Michelot,[1] Emmanuel Derivery,[1] Rajaa Paterski-Boujemaa,[1] Christophe Guérin,[1] Shanjin Huang,[2] François Parcy,[1] Christopher J. Staiger,[2] and Laurent Blanchoin[1,*]

[1] Departement Réponse et Dynamique Cellulaire
Laboratoire de Physiologie Cellulaire Végétale
Centre National de la Recherche Scientifique
Institut National de la Recherche Agronomique
Université Joseph Fourier
F38054 Grenoble
France

[2] Department of Biological Sciences and
The Bindley Bioscience Center
Purdue University
West Lafayette, Indiana 47907-2064

Summary

Actin-filament bundles (or cables) have a structural role during cell division and morphogenesis, but also serve as important "tracks" for the transport of materials during cytokinesis and polarized cell growth. However, the dynamic formation of these longitudinal actin-filament higher-order structures is not understood. Recently, several lines of evidence suggest that formins provide one avenue for the initiation of actin cables in vivo [1–3]. A popular model for the mechanism of polymerization of actin filaments by formin involves the processive movement of formin attached at the barbed end of an elongating filament [4]. In the present study, we use an in vitro system to reconstitute the dynamic formation of actin-filament bundles generated by *Arabidopsis* FORMIN1 (AFH1). To be able to visualize individual events in such a complex system, we used real-time evanescent-wave microscopy. Surprisingly, we find that AFH1 is a nonprocessive formin that moves from the barbed end to the side of an actin filament after the nucleation event. We show why this new mechanism of nucleation by a member of the formin family is important for bundle formation. Finally, we analyze the different parameters controlling the dynamic formation of such longitudinal actin-filament bundles.

Results

The Fluorescent Properties of Rhodamine- and Alexa-532-Labeled Actins Are Different

We used total-internal-reflection fluorescence microscopy (TIRFM) to study the dynamic formation of actin-filament bundles induced by *Arabidopsis* FORMIN1 (AFH1). We focused our study on AFH1, profilin, and actin because they are sufficient to reconstitute such structures in vitro [5]. To be able to distinguish individual molecular events in this complex system, in which overlapping reactions contribute to actin-bundle formation (including nucleation, elongation, and bundling), we used fluorescent actin that was labeled on lysine residues with rhodamine or Alexa dyes (Figures 1A and 1B; Movies S1 and S2 in the Supplemental Data available online). The Alexa-532-actin fluorescence intensity decreased rapidly as a result of photobleaching, generating actin filaments with a comet-like appearance (Figures 1B and 1C (bottom curve); Movie S2) where the subunits near the growing ends are always brighter (Figure 1B; Movie S2). By comparison, actin filaments generated with rhodamine-labeled monomers maintained a more homogenous fluorescence intensity over the same period of observation (i.e., 20 min; Figures 1A and 1C (top curve); Movie S1). Thus, Alexa-532-actin appears to be a useful probe for identifying and monitoring polymerization at the barbed end of actin filaments.

AFH1 Is a Nonprocessive Formin

We used both types of fluorescent actins bound to an excess of profilin to study the initial steps (i.e., nucleation and elongation) of filament assembly prior to actin-bundle formation. We focused our attention on actin filaments initiated by AFH1 at the surface of the cover glass by tracking filaments that remained attached by or near their end at the initial point of nucleation (Figures 2A and 2B; Movies S3 and S4). In this assay, it was possible to visualize multiple nucleation events from the same area ($\leq 0.012\ \mu m^2$) of the glass slide (red arrows, Figures 2A and 2B). This is characteristic of the nucleating activity of AFH1 (Figure 2; Movies S3 and S4; [5]). We were able to resolve each individual nucleation event when Alexa-532-labeled actin was polymerized in the presence of AFH1 (red arrow, Figure 2B; Movie S4). By analysis of the fluorescence intensity at the origin of nucleation (Figure 2B, red arrow), we obtained a perfect correlation between the number of fluorescent pulses (i.e., five) at the origin of nucleation (Figure 2C) and the number of actin filaments growing from this origin (Figure 2B, yellow arrows). These results indicate that, in some cases, there may be more than a dimer of AFH1 at the origin of nucleation allowing the ability to nucleate multiple actin filaments. Alternatively, each dimer of AFH1 may be capable of nucleating in succession several actin filaments. The distribution of nucleation events that were from the same origin and were analyzed from TIRFM experiments is similar for two different concentrations of AFH1 and typically ranged from 1 to 5 (Figure 2D), with a few larger structures representing less than 1% of the total events.

It is also instructive to consider the polarity of Alexa-532-labeled actin filaments generated by AFH1. Surprisingly, the brightest part of actin filaments (yellow arrows, Figure 2B; Movie S4), corresponding to the growing barbed ends, always moves away from the initial origin of nucleation (red arrow) as the filaments elongate at a rate of $8.1 \pm 1.2\ \mu M^{-1}\ s^{-1}$. The polarity of actin filaments

*Correspondence: laurent.blanchoin@cea.fr

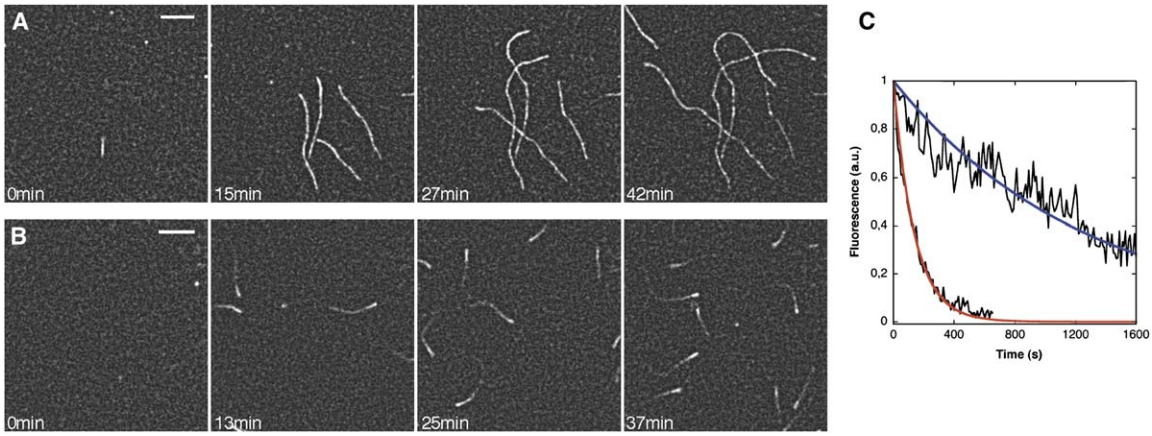

Figure 1. The Fluorescent Properties of Actin Filaments Labeled with Rhodamine or Alexa-532 Fluorophores Are Different

Conditions: NEM-myosin was attached to the cover glass before addition into the flow cell of 0.75 μM rhodamine-labeled actin or Alexa-labeled actin monomer in the presence of 1.5 μM profilin. Images were taken at the indicated time during polymerization.

(A) Time-lapse evanescent-wave microscopy of rhodamine-labeled actin polymerization. The stability of the fluorophore bound to actin enabled us to visualize the whole polymerization process as well as the resulting actin filaments.

(B) Time-lapse evanescent-wave microscopy of Alexa-532-labeled actin polymerization. The comet-like appearance of actin filaments is due to the photobleaching of the fluorophore. We were able to follow only the newly polymerized part of the filaments. This does, however, favor the identification of the growing barbed ends.

(C) Variation of the fluorescence intensity over time for both labeled actins under TIRFM. The typical photobleaching time scale is ten times longer for rhodamine actin (top "noisy" curve) than for Alexa-532 actin (bottom "noisy" curve) as determined by the exponential decay of fluorescence (blue curve for rhodamine actin, red curve for Alexa-532 actin).

Scale bars represent 5 μm.

generated by AFH1 was identical regardless of whether a single or multiple nucleating events occurred from the same site (data not shown). This is different from nucleation by a processive formin, such as mDia2, where the brightest part of the filament remains at the origin of nucleation (red arrow, Movie S5; e.g., [6]). Indeed, with a processive formin, labeled actin monomers are continuously inserted between the actin-filament barbed end and the formin attached at the glass slide ([6]; Movies S5 and S6). Moreover, all processive formins tested until now modify the rate of elongation at the barbed ends of actin filaments in the presence of profilin ([7, 8]; Movie S6). In our case, the rate of elongation at the barbed ends was similar for actin filaments nucleated in the presence or absence of AFH1: k+ = 7.8 ± 1.2 μM^{-1} s^{-1} for Alexa-532-labeled actin bound to profilin (Figure 1B) and k+ = 8.1 ± 1.2 μM^{-1} s^{-1} for Alexa-532-labeled actin bound to profilin in presence of AFH1 (Figure 2B). By comparison, the rate of elongation increased from k+ = 5.9 ± 0.7 μM^{-1} s^{-1} for rhodamine actin bound to profilin up to k+ = 24.5 μM^{-1} s^{-1} for rhodamine actin bound to profilin in the presence of mDia1 (Movie S6). Finally, the presence of both NEM-myosin and processive formins (mDia1 or mDia2) attached to the cover glass often induces a buckling of actin filaments ([6]; Movies S5 and S6). No buckling events were observed for AFH1 [5]. An elongation assay performed in the presence of capped barbed ends shows that AFH1 does not bind to filament pointed ends (Figure S2). This discounts the possibility that AFH1 is nucleating like the Arp2/3 complex, i.e., remaining attached to pointed ends. Moreover, annealing events can be observed on elongating filaments generated by AFH1 in agreement with AFH1 not "surfing" at the elongated barbed end of an actin filament (Figure 2A, pink arrows; Movie S4).

AFH1 Attached to the Side of a Pre-existing Actin Filament Is Able to Nucleate New Filaments

The nonprocessivity of AFH1 may be explained by its high affinity for the side of actin filaments (K_d = 0.13 μM; [5]). To better understand the mechanism of action of AFH1, we determined whether AFH1 bound to the side of an actin filament was able to nucleate new actin filaments. After the addition of rhodamine-labeled actin monomers bound to profilin, we observed dense polymerization from AFH1 bound to pre-existing filaments, whereas almost no polymerization was detected on other parts of the slide (Figure 3A; Movie S7). This strongly suggests that AFH1 bound to actin filaments is able to nucleate new actin filaments. Using pyrene fluorescence, we confirmed this hypothesis by a kinetic-polymerization assay from actin seeds. The polymerization of pyrene-labeled actin monomers from a mixture of actin filaments or actin filaments bound to *Arabidopsis* VILLIN1 (another actin-filament side-binding protein but with no nucleating activity; [9]) elongated at the same rate (Figure 3B). However, the polymerization is faster when actin filaments are incubated with AFH1 (Figure 3B). This is consistent with AFH1 being an active nucleator when bound to the side of a pre-existing actin filament.

The use of Alexa-532-labeled actin allowed us to visualize individual nucleation events (red arrow, Figure 4C) during the polymerization of actin filaments from Alexa-532-phalloidin-labeled actin filaments decorated with AFH1 (Figure 4B: Movie S12). Actin filaments nucleated from the side of the pre-existing filaments have their brightest ends (yellow arrows, Figure 4B) moving away from the origin of nucleation on the pre-existing filaments (red arrow, Figure 4B), in agreement with the nonprocessivity of AFH1.

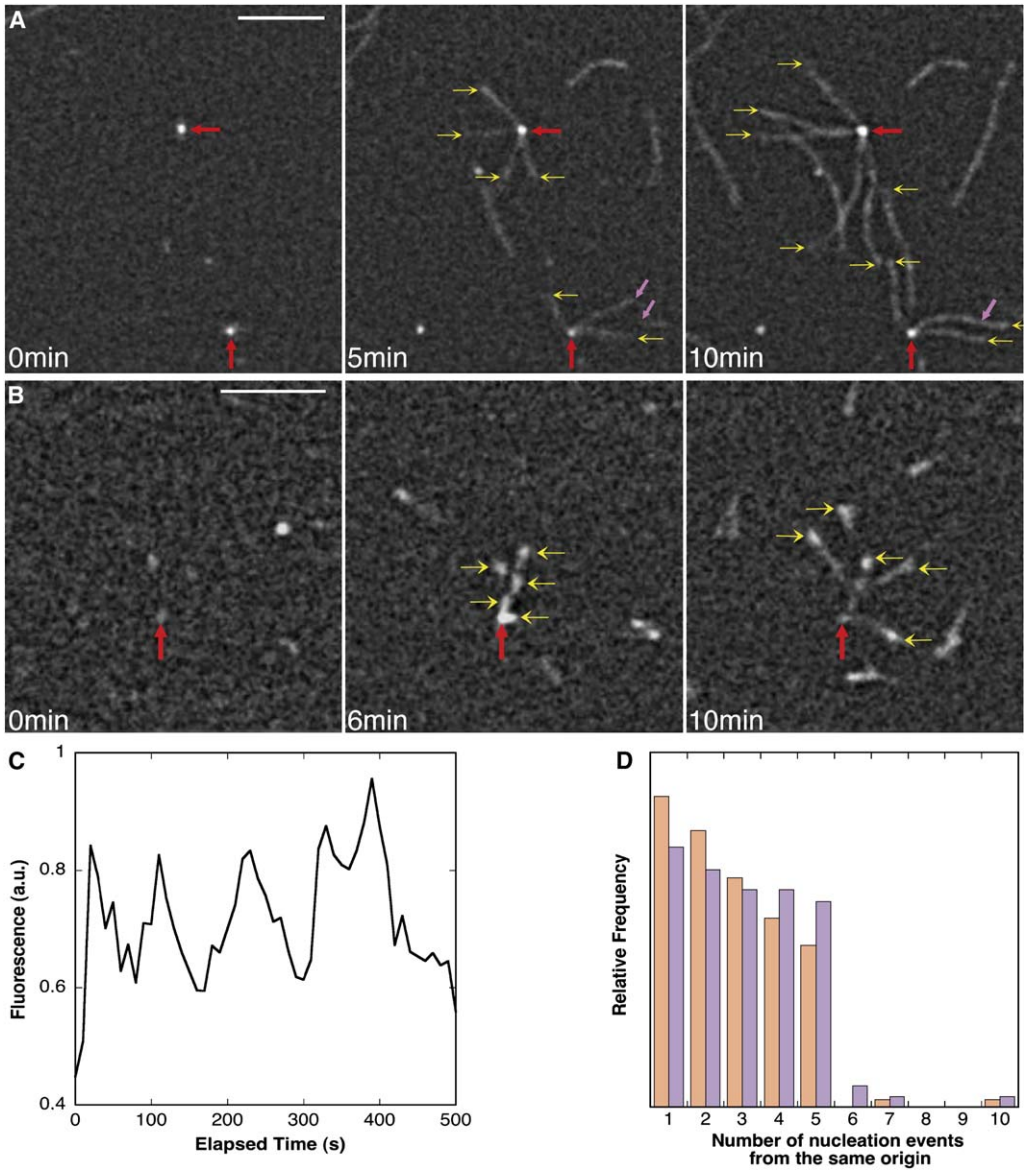

Figure 2. AFH1 Is a Nonprocessive Formin

Conditions: AFH1, FH1-FH2-Cter (40 nM), was attached to the cover glass before addition into the flow cell of 0.75 μM rhodamine- or Alexa-532-labeled actin monomer in the presence of 1.5 μM profilin. Images were taken at the indicated time during polymerization.

(A) Time-lapse evanescent-wave microscopy of rhodamine-labeled actin polymerization in the presence of AFH1. The origin of nucleation by AFH1 is indicated by a red arrow. Filaments that have grown out from the origin of nucleation are indicated by yellow arrows. The rates of elongation for these filaments are typical of barbed-end growth (i.e., 8.1 μM^{-1} s^{-1}), and an annealing event is visible at the elongating barbed end of an actin filament (pink arrows).

(B) Time-lapse evanescent-wave microscopy of Alexa-532-actin polymerization in the presence of AFH1. Actin-filament barbed ends (yellow arrows) are moving away from the initial origin of nucleation (red arrow), showing the nonprocessive behavior of AFH1.

(C) Quantification of fluorescence intensity at the origin of nucleation (red arrow in [B]) enables us to distinguish five consecutive pulses of fluorescence corresponding to five nucleation events and the five resulting actin filaments in [B].

(D) Quantification of the relative frequency of nucleation events from the same origin of nucleation. Differently colored bars represent two different concentrations of AFH1 attached to the cover glass in independent experiments (orange, 40 nM AFH1 and purple, 100 nM). This distribution was similar for AFH1, GST-FH1-FH2-His, and His-FH1-FH2-His constructs, ruling out a possible effect of GST on the behavior of AFH1.

Scale bars in (A) and (B) represent 5 μm.

To visualize the location of AFH1 during nucleation and subsequent elongation events, we incubated rhodamine-phalloidin-labeled actin filaments with a construct where AFH1 is fused to green fluorescence protein (GFP). At steady state, GFP-AFH1 associated with actin-filament bundles at numerous locations (Figure 3C). By TIRFM, we observed that GFP-AFH1 remains bound to the side of the pre-existing filaments after nucleation of new filaments (Figure 3D; Movie S8), consistent with nonprocessivity and with the ability of AFH1 to simultaneously bind the side of filaments and nucleate.

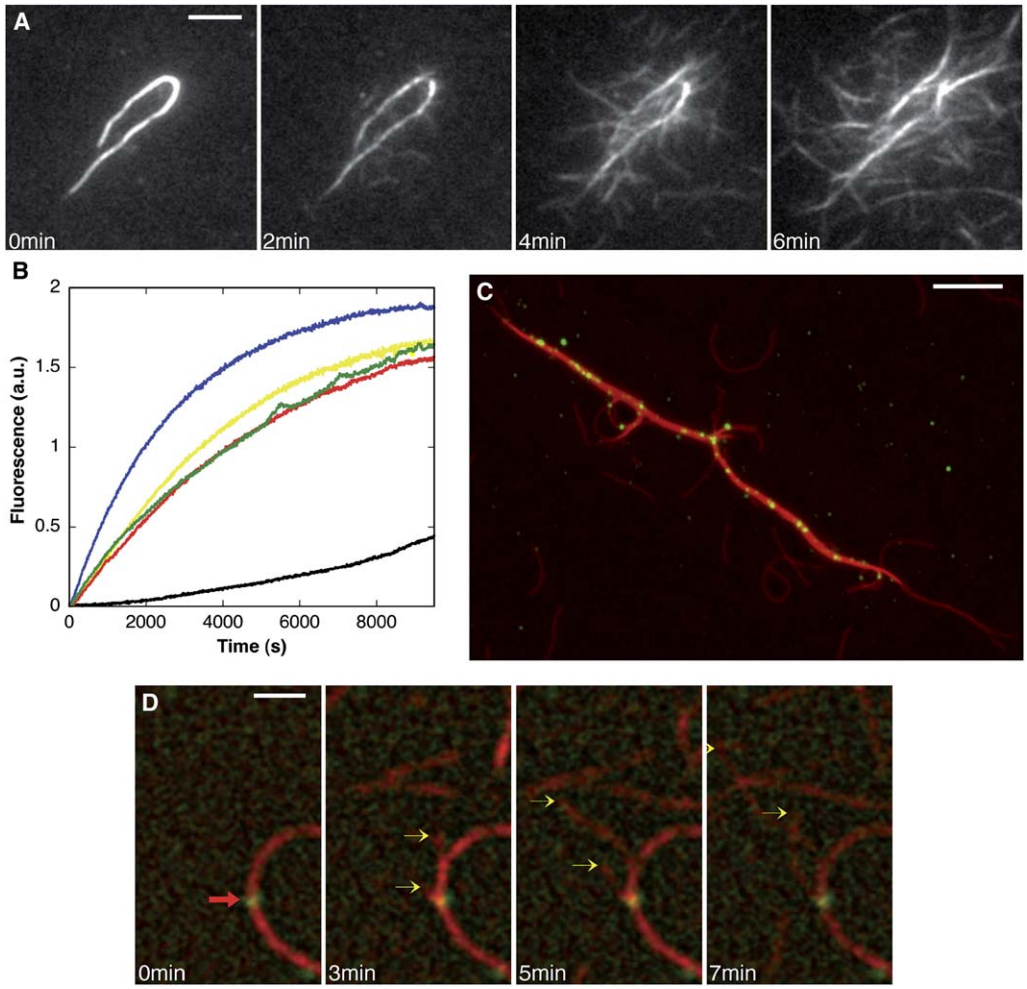

Figure 3. AFH1 Has Nucleation Activity When Bound to the Side of an Actin Filament

(A) AFH1 is able to nucleate new filaments from the sides of a pre-existing filament. Conditions: Alexa-532-phalloidin-labeled actin filaments (180 nM) were incubated for 30 s with 50 nM AFH1 and then immobilized on the coverslip of a flow cell blocked with 1% BSA. Polymerization was initiated by the addition of 0.75 μM actin monomers (rhodamine-labeled) and 1.5 μM profilin. Images were taken at the indicated time during polymerization. Numerous polymerization events were observed from the pre-existing filaments decorated with AFH1, whereas almost no polymerization was observed on the surrounding part of the cover glass.

(B) AFH1 nucleates actin-filament formation with the same efficiency whether it is free or bound to pre-existing filaments. To demonstrate that AFH1 bound to filaments was able to nucleate filaments with the same efficiency as free AFH1, we conducted pyrene-actin polymerization assays with 2 μM actin and 2 μM profilin alone (black), with 10 nM AFH1 (yellow), with 50 nM phalloidin filaments (red), with 50 nM phalloidin filaments and 10 nM AtVILLIN1 (green), or with 50 nM phalloidin filaments and 10 nM AFH1 (blue). The concentration of actin-filament barbed ends generated from each experiment was 0.016 nM for 10 nM AFH1 alone, 0.014 nM for 50 nM phalloidin actin filaments, 0.016 nM for 50 nM phalloidin actin filaments with 10 nM AtVILLIN1, and 0.034 nM for 50 nM phalloidin actin filaments with 10 nM AFH1.

(C) Direct visualization of actin-filament bundles decorated with GFP-AFH1. Actin was polymerized with GFP-AFH1 for 30 min in the presence of rhodamine phalloidin and then diluted to 10 nM before observation with wide-field fluorescence microscopy.

(D) GFP-AFH1 can nucleate new actin filaments when bound to the side of a pre-existing filament. Rhodamine-phalloidin-labeled actin filaments (180 nM) were preincubated with 50 nM GFP-AFH1 and then immobilized on the cover glass of the flow cell before addition of 0.75 μM rhodamine-labeled actin and 1.5 μM profilin. By rapidly switching between laser illumination of the evanescent wave (to observe polymerization) and wide-field fluorescence microscopy (to visualize GFP-AFH1), we were able to monitor actin-filament growth (yellow arrows) at a rate of elongation = 8 ± 1 μM^{-1} s^{-1} from GFP-AFH1 (red arrow) bound to the side of pre-existing filaments.

Scale bars represent 5 μm in (A) and (C) and 2 μm in (D).

AFH1 Induces Actin-Bundle Formation by Promoting the "Zippering" of Actin Filaments

We next studied the dynamic formation of actin bundles generated by AFH1 (Figures 4A and 4B; Movies S9, S11, and S12). The bundling activity of AFH1 depends upon the presence of an FH1 domain [5]; however, FH1 domain alone does not bind actin monomers or filaments (data not shown). Three events are particularly clear during the kinetic formation of actin bundles. First, the fluorescence intensity of the original actin filament increased dramatically over time, in agreement with the continuous nucleation of new actin filaments by AFH1 attached to the side of the pre-existing actin filament (Figure 4A; Movie S9). Second, the formation of actin bundles required a "zippering" event near the tip of growing barbed ends of actin filaments (Figure 4A,

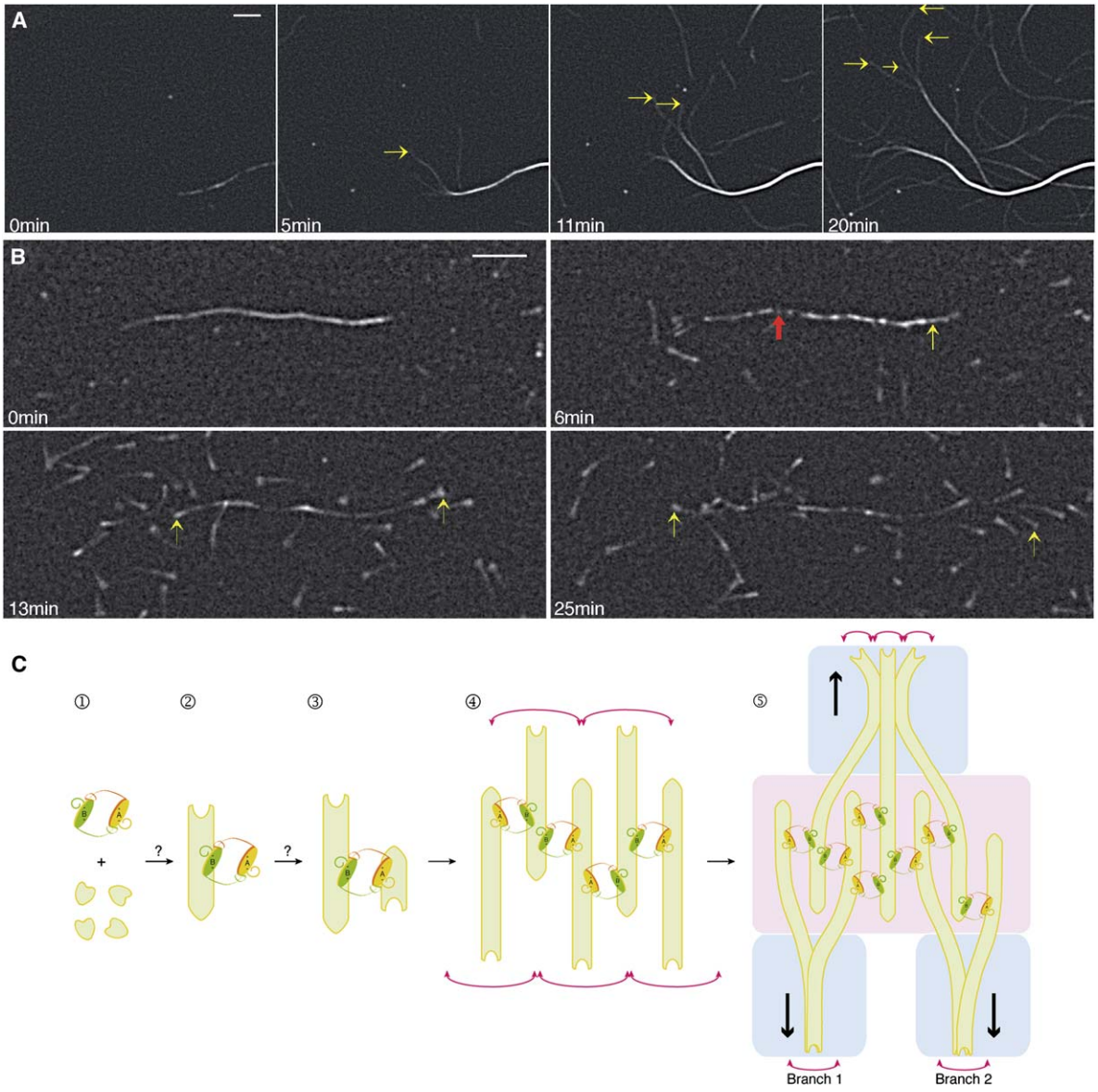

Figure 4. Dynamic Formation of Actin-Filament Bundles by AFH1

Conditions: Rhodamine-phalloidin-labeled actin filaments (180 nM) were incubated with 50 nM AFH1 and then immobilized on the coverslip of a flow cell blocked with 1% BSA. To allow filament assembly, we added 0.75 μM actin monomers (rhodamine-labeled) and 1.5 μM profilin to the flow cell. Images were taken at the indicated time during polymerization.

(A) Time-lapse evanescent-wave microscopy of the formation of actin bundles by AFH1. A wave of fluorescent filaments emanates from the pre-existing actin filament consistent with actin nucleation by AFH1 bound to the original actin filament. Zippering of actin filaments occurs near the growing barbed ends (yellow arrows) and favors actin-filament-bundle formation.

(B) Alexa-532-labeled actin allowed us to understand the mechanism of formation of actin bundles. Conditions: Alexa-532-phalloidin-labeled actin filaments (180 nM) were pre-incubated with 50 nM AFH1 and then immobilized on the coverslip of a flow cell blocked with 1% BSA. To allow assembly, we added 0.75 μM actin monomers (Alexa-532-labeled) and 1.5 μM profilin. AFH1 favors a "clustered" nucleation of actin filaments (red arrow) that are subsequently zippered together (yellow arrows) while elongating. This zippering effect leads to a random organization of actin filaments in the nucleation zone, but favors a parallel actin-filament organization away from the origin of nucleation. The rates of elongation for individual actin filaments before their integration into the bundle or when extending along another actin filament were the same (i.e., 5.5 ± 1.5 $\mu M^{-1}\ s^{-1}$), suggesting that the growth of actin filaments inside the bundles was not sterically limited.

Scale bars represent 5 μm.

(C) Model for the dynamic formation of actin bundles by nonprocessive FORMIN1 (AFH1). We propose that AFH1 moves from the end to the side of an actin filament after nucleation by an uncharacterized mechanism (steps 1 and 2). AFH1 bound to the side of a pre-existing filament can nucleate a new actin filament (step 3) and organizes actin filaments into bundles (steps 4 and 5). Thermal fluctuations favor filament-filament interaction (red arrows, step 4). However, the stiffness of actin-filament structure inhibits the amplitude of the thermal fluctuation (decreased size of red arrows, step 5) and induces branch formation (step 5). The direction of the zippering follows actin-filament elongation (black arrows, step 5). Actin bundles are in antiparallel orientation near the origin (pink zones, step 5) of nucleation and in parallel orientation away from the origin of nucleation (blue zone, step 5).

yellow arrows; Movie S9). Third, this zippering of actin filaments is promoted by AFH1 that favors a "clustered" nucleation of actin filaments (Figures 4A and 4B) and by the Brownian motion that promotes actin-filament contact (Figure 4A, yellow arrows; Movie S9). Similar experiments done with mammalian mDia2 demonstrate that mDia2 is able to generate actin bundles, in agreement with a previous report [10]. Like AFH1, mDia2 is able to nucleate a new actin filament when bound to the side of a pre-existing filament. Distinct from AFH1, mDia2 generates actin filaments that buckle, consistent with it being processive while bound to the side of a pre-existing filament (Movie S10).

AFH1 Organizes Actin Filaments into Antiparallel and/or Parallel Bundles

The use of Alexa-532 actin was crucial for studying the polarity of individual actin filaments during the formation of bundles. Specifically, the rapid decrease of the fluorescence from Alexa-532 actin enabled us to follow the growth of individual actin filaments inside or along the actin bundles (Figure 4B, yellow arrows; Movie S12). The brightest parts of actin filaments, corresponding to the elongating barbed ends (rate of elongation, 5.5 ± 1.5 μM^{-1} s^{-1}), were observed to pass each other near the origin of nucleation, suggesting that some of the actin filaments that form actin bundles were in antiparallel orientation (Figure 4B; Movie S12). However, as actin filaments elongated, all the barbed ends were growing away from the origin of nucleation generating parallel bundles (Figure 4B; Movie S12). During the full process of actin-filament-bundle formation, no sliding of polymerized filaments was observed, suggesting that actin filaments are crosslinked at least at the original point of nucleation.

Discussion

This study reports on a unique mechanism for a member of the formin family of actin nucleators. Remarkably, after nucleation of an actin filament, AFH1 does not remain attached to the growing barbed end as would be expected for a processive nucleator, but rather it moves to the side of the actin filament, thereby releasing the barbed end. This behavior is independent of the presence of profilin (data not shown). We suggest that this mechanism of action is favored by the strong affinity of AFH1 for the side of an actin filament (K_d = 0.13 μM; [5]). AFH1 does bind with a higher affinity to the actin-filament barbed end (K_d = 40 nM; [5]); however, the concentration of barbed ends is at least an order of magnitude lower than the concentration of binding sites along the side of an actin filament. AFH1-FH1-FH2 was unable to completely block assembly at filament barbed ends in an elongation assay or inhibit capping by *Arabidopsis* capping protein (AtCP) (Figure S2; [5]). Moreover, its nucleation activity is completely abolished in the presence of an equimolar amount of capping protein, consistent with weak or transient binding to filament barbed ends [5]. From the current work, we cannot make any firm conclusions about the exact mechanism of nucleation by AFH1, because the resolution of the TIRFM assay is around 0.5 μm (about 166 subunits long). AFH1 may act as a processive formin in an early step (i.e., actin filaments less than ≈100 subunits long) and then slides to the side in a time scale not observable in our assay. Other formins including mammalian FRL1 and mDia2 [10] and yeast Bnr1 [11] have been shown to bind to the side and generate filament bundles. However, the affinity for the interaction with the side of an actin filament varies substantially, from the tight binding of AFH1 and FRL1, (K_d ~0.1 μM; [12]) to the weak binding of mDia1 (K_d ~3 μM; [12]). Recent work suggests that FRL1 shares the same region for side binding and end binding, whereas mDia2 has different regions responsible for each activity [10]. We report here that mDia2 is still processive when bound to the side of an actin filament (Movie 10). However, we cannot exclude in the case of mDia2 that the side binding may affect quantitatively its nucleating activity and/or processivity, in which case the importance of the side-binding versus processive nucleation needs further investigation. Obviously more works need to be done on the structural relationship between filament side binding, nucleation, and processive elongation. Nevertheless, AFH1 seems to be the first example of a formin family member that does not exhibit processive behavior at filament ends.

The direct visualization with TIRFM of bundle formation by AFH1 provides insight into the tight relationship between nonprocessivity and the mechanism of bundle formation. We have developed a simple model (Figure 4C) that predicts a general mechanism for the dynamic formation of actin bundles. The mechanism of bundle formation proposed for AFH1 is somewhat similar to a model for the formation of filopodia-like bundles in vitro and in vivo [13, 14]. However, the model for filopodia-like bundles requires tight coordination between an activated nucleator (Arp2/3 complex) and a bundler (fascin). Here, a single protein accomplishes both functions. Two important physical phenomena may contribute to the zippering mechanism (Figure 4C, black arrows) and will affect the bundling efficiency independent of the presence of actin-binding proteins. First, the Brownian motion, which induces thermal fluctuations of the growing ends, possibly favors to some extent the filament-filament interaction (Figure 4C, red arrows). Further, we might imagine that if the thermal fluctuations of actin filaments are too great, actin filaments coming into contact with each other may break or dissociate from the bundles. Second, the overall flexibility of an actin filament is a potential determinant of bundle formation. Our results suggest that there is a critical stiffness of actin filaments organized into bundles above which thermal fluctuations are too weak to induce the zippering. The resulting effect is the generation of thick branches from the original bundles (Figure 4C, Step 5, branches 1 and 2).

Using Alexa-532-labeled actin, we determined that actin bundles have a random polarity at the origin of nucleation (Figure 4C, pink zones), but as actin filaments elongate, all barbed ends become oriented in the same direction at both ends of the bundles (Figure 4C, blue zone). The overall polarity of bundles is therefore mostly parallel. FRL1 and mDia2 generate bundles with a random orientation [10].

The use of Alexa-532 actin in TIRFM will be of a great interest in the future to study the dynamic behavior of higher-order actin-based structures. For example, this probe could facilitate understanding of the coordination

between bundles of actin filaments generated by formins and actin-filament networks generated by Arp2/3 complex. Finally, we should pay particular attention to the role of contractile proteins in the regulation of the dynamic formation of higher-order actin-filament arrays. As a starting point, we report here that interaction of actin bundles with myosin II is a possible mechanism for bundle dissociation (Movie S11).

Supplemental Data

Supplemental Data include Experimental Procedures, two figures, and twelve movies and are available with this article online at: http://www.current-biology.com/cgi/content/full/16/19/1924/DC1/.

Acknowledgments

We thank Dr. Robert Robinson for his advice on the model of actin-filament bundling by AFH1. We are grateful to Dr. Henry N. Higgs for providing mammalian formins and for performing analytical ultracentrifugation experiments with AFH1. This work was funded through grants from the Actions Thématiques et Initiatives sur Programmes et Equipes Plus (ATIP+) and Contract Plan Epargne Région to L.B. and from the National Research Initiative of the USDA Cooperative State Research, Education, and Extension Service, grant number 2002-35304-12412 to C.J.S.

Received: April 20, 2006
Revised: June 28, 2006
Accepted: July 21, 2006
Published: October 9, 2006

References

1. Evangelista, M., Zigmond, S., and Boone, C. (2003). Formins: Signaling effectors for assembly and polarization of actin filaments. J. Cell Sci. *116*, 2603–2611.
2. Sagot, I., Rodal, A.A., Moseley, J., Goode, B.L., and Pellman, D. (2002). An actin nucleation mechanism mediated by Bni1 and profilin. Nat. Cell Biol. *4*, 626–631.
3. Kobielak, A., Pasolli, H.A., and Fuchs, E. (2004). Mammalian formin-1 participates in adherens junctions and polymerization of linear actin cables. Nat. Cell Biol. *6*, 21–30.
4. Zigmond, S.H., Evangelista, M., Boone, C., Yang, C., Dar, A.C., Sicheri, F., Forkey, J., and Pring, M. (2003). Formin leaky cap allows elongation in the presence of tight capping proteins. Curr. Biol. *13*, 1820–1823.
5. Michelot, A., Guerin, C., Huang, S., Ingouff, M., Richard, S., Rodiuc, N., Staiger, C.J., and Blanchoin, L. (2005). The formin homology 1 domain modulates the actin nucleation and bundling activity of Arabidopsis FORMIN1. Plant Cell *17*, 2296–2313.
6. Kovar, D.R., and Pollard, T.D. (2004). Insertional assembly of actin filament barbed ends in association with formins produces piconewton forces. Proc. Natl. Acad. Sci. USA *101*, 14725–14730.
7. Romero, S., Le Clainche, C., Didry, D., Egile, C., Pantaloni, D., and Carlier, M.F. (2004). Formin is a processive motor that requires profilin to accelerate actin assembly and associated ATP hydrolysis. Cell *119*, 419–429.
8. Kovar, D.R., Harris, E.S., Mahaffy, R., Higgs, H.N., and Pollard, T.D. (2006). Control of the assembly of ATP- and ADP-actin by formins and profilin. Cell *124*, 423–435.
9. Huang, S., Robinson, R.C., Gao, L.Y., Matsumoto, T., Brunet, A., Blanchoin, L., and Staiger, C.J. (2005). Arabidopsis VILLIN1 generates actin filament cables that are resistant to depolymerization. Plant Cell *17*, 486–501.
10. Harris, E.S., Rouiller, I., Hanein, D., and Higgs, H.N. (2006). Mechanistic differences in actin bundling activity of two mammalian formins, FRL1 and mDia2. J. Biol. Chem. *280*, 14383–14392.
11. Moseley, J.B., and Goode, B.L. (2005). Differential activities and regulation of S. cerevisiae formins Bni1 and Bnr1 by Bud6. J. Biol. Chem. *280*, 28023–28033.
12. Harris, E.S., Li, F., and Higgs, H.N. (2004). The mouse formin, FRLalpha, slows actin filament barbed end elongation, competes with capping protein, accelerates polymerization from monomers, and severs filaments. J. Biol. Chem. *279*, 20076–20087.
13. Vignjevic, D., Yarar, D., Welch, M.D., Peloquin, J., Svitkina, T., and Borisy, G.G. (2003). Formation of filopodia-like bundles in vitro from a dendritic network. J. Cell Biol. *160*, 951–962.
14. Haviv, L., Brill-Karniely, Y., Mahaffy, R., Backouche, F., Ben-Shaul, A., Pollard, T.D., and Bernheim-Groswasser, A. (2006). Reconstitution of the transition from lamellipodium to filopodium in a membrane-free system. Proc. Natl. Acad. Sci. USA *103*, 4906–4911.